# Electrochemical Engineering Applications

*Ralph E. White, Robert F. Savinell and Alfred Schneider, editors*

AIChE Symposium Series

254 *Volume 83, 1987*

ERICAN INSTITUTE OF CHEMICAL ENGINEERS

# Electrochemical Engineering Applications

*Ralph E. White,*
*Robert F. Savinell and Alfred Schneider,*
*editors*

R.P. Allen
M.M. Baizer
D.M. Black
L.A. Bray
G.W. Brutchen
L. Burris
Y.-C. Chang
S.-L. Chiu
A.P. David
S.J. Dukas
M.A. Ebra
J.F. Fatula
S.D. Fritts
R.L. Galyen
H. Goldacker
H. Gu
K.-C. Ho
D.T. Hobbs
E. Hyman
J. Jorne
K. Kanari
H.F. Leibecki
L.W. McClure
J.N. Michaels
W.E. Miller
K. Nobe
K. Nozaki
G.F. Offutt
M.E. Orazem
R.A. Oriani
T. Ozawa
N. Phan
P.N. Pintauro
G. Prentice
J.D. Reid
A. Robbat
N.L. Robertson
J.L. Ryan
R.F. Savinell
H. Schmieder
S. Seimanides
J.R. Selman
W.C. Spindler
R.K. Steunenberg
M. Stoukides
J.B. Talbot
E.J. Wheelwright

AIChE Symposium Series

Number 254 1987 Volume 83

*Published by*

American Institute of Chemical Engineers

345 East 47 Street New York, New York 10017

**Library of Congress Cataloging-in-Publication Data**
Electrochemical engineering applications.

(AIChE symposium series ; no. 254, v. 83)
Based on papers presented at the AIChE Annual meeting in Miami, November 1986.
Includes index.
1. Electrochemistry, Industrial—Congresses.
I. White, Ralph E. II. Savinell, Robert F., 1950- III. Schneider, Alfred, 1926- . IV. American Institute of Chemical Engineers. Meeting (1986 : Miami, Fla.) V. Series: AIChE symposium series ; no. 254.
TP250.E48 1987 660.2'97 87-11555
ISBN 0-8169-0405-7



Printed in the United States of America by
Twin Production & Design

# SYMPOSIUM SERIES

## ADSORPTION

- 96 Developments in Physical Adsorption
- 117 Adsorption Technology
- 219 Recent Advances in Adsorption and Ion Exchange
- 230 Adsorption and Ion Exchange—'83
- 233 Adsorption and Ion Exchange—Progress and Future Prospects
- 242 Adsorption and Ion Exchange: Recent Developments

## AEROSPACE

- 33 Rocket and Missile Technology
- 52 Chemical Engineering Techniques in Aerospace

## BIOENGINEERING

- 69 Bioengineering and Food Processing
- 84 The Artificial Kidney
- 86 Bioengineering ... Food
- 93 Engineering of Unconventional Protein Production
- 99 Mass Transfer in Biological Systems
- 108 Food and Bioengineering—Fundamental and Industrial Aspects
- 114 Advances in Bioengineering
- 163 Water Removal Processes: Drying and Concentration of Foods and Other Materials
- 172 Food, pharmaceutical and bioengineering—1976/77
- 181 Biochemical Engineering Renewable Sources of Energy and Chemical Feedstocks

## CRYOGENICS

- 224 Cryogenic Processes and Equipment 1982
- 251 Cryogenic Properties, Processes and Applications 1986

## CRYSTALLIZATION

- 110 Factors Influencing Size Distribution
- 193 Design Control and Analysis of Crystallization Processes
- 215 Nucleation, Growth and Impurity Effects in Crystallization Process Engineering
- 240 Advances in Crystallization From Solutions
- 253 Fundametnal Aspects of Crystallization and Precipitation Processes

## DRAG REDUCTION

- 111 Drag Reduction
- 130 Drag Reduction in Polymer Solutions

## ENERGY

### Conversion and Transfer

- 5 Heat Transfer, Atlantic City
- 57 Heat Transfer, Boston
- 59 Heat Transfer, Cleveland
- 75 Energy Conversion Systems
- 79 Heat Transfer with Phase Change
- 87 Advances in Cryogenic Heat Transfer
- 113 Convective and Interfacial Heat Transfer
- 118 Heat Transfer—Tulsa
- 119 Commercial Power Generation
- 138 Heat Transfer—Research and Design
- 162 Energy and Resource Recovery from Industrial and Municipal Solid Wastes
- 174 Heat Transfer: Research and Application
- 189 Heat Transfer—San Diego 1979
- 202 Transport with Chemical Reactions
- 208 Heat Transfer—Milwaukee 1981
- 216 Processing of Energy and Metallic Minerals
- 225 Heat Transfer—Seattle 1983
- 236 Heat Transfer—Niagara Falls 1984

### Nuclear Engineering

- 53 Part XIII
- 56 Part XIV
- 94 Part XX
- 104 Part XXI
- 106 Part XXII
- 119 Commercial Power Generation
- 168 Heat Transfer in Thermonuclear Power Systems
- 169 Developments in Uranium Enrichment
- 191 Nuclear Engineering Questions Power Reprocessing, Waste, Decontamination Fusion
- 221 Recent Developments in Uranium Enrichment

## ENVIRONMENT

- 78 Water Reuse
- 97 Water—1969
- 115 Important Chemical Reactions in Air Pollution Control
- 122 Chemical Engineering Applications of Solid Waste Treatment
- 124 Water—1971
- 126 Air Pollution and its Control
- 133 Forest Products and the Environment
- 137 Recent Advances in Air Pollution Control
- 139 Advances in Processing and Utilization of Forest Products
- 144 Water—1974: I. Industrial Wastewater Treatment
- 145 Water—1974: II. Municipal Wastewater Treatment
- 146 Forest Product Residuals
- 147 Air: I. Pollution Control and Clean Energy
- 148 Air: II. Control of $NO_{xx}$ and $SO_x$ Emissions
- 149 Trace Contaminants in the Environment
- 151 Water—1975
- 156 Air Pollution Control and Clean Energy
- 157 New Horizons for the Chemical Engineer in Pulp and Paper Technology
- 165 Dispersion and Control of Atmospheric Emissions, New-Energy-Source Pollution Potential
- 170 Intermaterials Competition in the Management of Shrinking Resources
- 171 What the Filterman Needs to Know About Filtration
- 175 Control and Dispersion of Air Pollutants: Emphasis on $NO_x$ and Particulate Emissions
- 177 Energy and Environmental Concerns in the Forest Products Industry
- 184 Advances in the Utilization and Processing of Forest Products
- 188 Control of Emissions from Stationary Combustion Sources Pollutant Detection and Behavior in the Atmosphere
- 195 The Role of Chemical Engineering in Utilizing the Nation's Forest Resources
- 196 Implications of the Clean Air Amendments of 1977 and of Energy Considerations for Air Pollution Control
- 198 Fundamentals and Applications of Solar Energy
- 200 New Process Alternatives in the Forest Products Industries
- 201 Emission Control from Stationary Power Sources: Technical, Economic and Environmental Assessments
- 207 The Use and Processing of Renewable Resources—Chemical Engineering Challenge of the Future
- 209 Water—1980
- 210 Fundamentals and Applications of Solar Energy II
- 211 Research Trends in Air Pollution Control: Scrubbing, Hot Gas Clean-up, Sampling and Analysis
- 213 Three Mile Island Cleanup
- 223 Advances in Production of Forest Products
- 232 Applications of Chemical Engineering in the Forest Products Industry
- 235 Impact of Energy and Environmental Consideration on Chemical Engineering in the Forest Products Industry
- 243 Separation of Heavy Metals and Other Trace Contaminants
- 244 Advances in Process Analysis and Development in the Forest Products Industries.

## FLUIDIZATION

- 101 Fundamental Processes in Fluidized Beds
- 105 Fluidization Fundamentals and Application
- 116 Fluidization: Fundamental Studies Solid-Fluid Reactions, and Applications
- 176 Fluidization Application to Coal Conversion Processes
- 205 Recent Advances in Fluidization and Fluid-Particle Systems
- 238 Fluidization and Fluid Particle Systems: Processes and Applications
- 241 Fluidization and Fluid Particle Systems: Recent Advances

## FOREWORD

Electrochemical engineering has become a more quantitative discipline during the past two to three decades because scientists have made great strides in understanding electrochemical phenomena. The structure of the double-layer, the phenomena of adsorption, desorption, and charge transfer are all being elucidated. These events and the resulting cross-fertilization have lead to a more rational and quantitative way of designing and optimizing electrochemical processes. Organizers for Area 1e of the AIChE, Electrochemical Fundamentals, have been responsive to the need to disseminate the progress being made in this dynamic field.

This volume consists of a number of papers presented at a symposium consisting of six sessions of the AIChE Fall Annual Meeting, November 2-7, 1986, in Miami Beach, Florida. Papers are reported that relate fundamental electrochemistry and industrial electrochemical processes. Two sessions included a number of mathematical models of batteries and fuel cells of practical interest. Although mathematical modeling and simulation have made significant improvements in cell design, the models do need basic information about the kinetics of industrial reactions. Therefore, three sessions were organized on this topic. Finally, one session was dedicated to the application of electrochemistry in the nuclear industry.

This volume highlights some of the advances being made in applying engineering and scientific principles to understanding industrial electrolytic systems. We hope this Symposium Series Volume will be a useful reference to those involved in this effort.

Ralph E. White
Department of Chemical Engineering
Texas A&M University
College Station, TX

Robert F. Savinell
Department of Chemical Engineering
Case Western Reserve University
Cleveland, OH

Alfred Schneider
Nuclear Engineering Department
Georgia Institute of Technology
Atlanta, GA

# INDEX


A

Applications ..... 78

B

Batteries ..... 46
Battery ..... 78,87,92

C

Cathodic-anodic overpotential ..... 40
Cells ..... 46
Computer model ..... 143
Computer simulation ..... 104
Corrosion ..... 15,25,64,111
Current distribution ..... 96
Current interruption methode ..... 40

D

Decontamination ..... 149
Deposit morphology ..... 15
Design ..... 92
Dissolution ..... 120,128
Dynamics ..... 64

E

Electro-organic ..... 34
Electro-synthesis ..... 34
Electrochemical ..... 64,120
Electrode kinetics ..... 9
Electrode passivation ..... 1
Electrodeposition process ..... 1
Electrolysis ..... 143,149
Electrolytic ..... 128
Electropolishing ..... 156
Electrorefining ..... 135

F

Fission products ..... 135
Fuel cell ..... 96
Fuel reprocessing ..... 135

H

H-cell ..... 34
Headend ..... 128
Hydrogen-bromine ..... 96

I

IFR ..... 135
Impedance ..... 92
Impregnation ..... 87

K

Kinetics of copper dissolution ..... 1

L

Lead-acid ..... 78
Life projections ..... 46
Limiting current ..... 56

M

Mass transfer ..... 15
Mathematical model ..... 9,25,96
Mechanism ..... 9
Membrane ..... 96
Methane oxidation ..... 40
Mixer settler ..... 143
Model ..... 78
Modeling ..... 46,64,92

N

Nickel-hydrogen ..... 46
Nickel batteries ..... 87
Nickel electrode ..... 87
Nitrate ..... 149
Nitrite ..... 149
Numerical analysis ..... 15,111

O

Oscillations ..... 64
Oxygen exchange kinetics ..... 56
Oxygen free copper anodes ..... 1

P

Parameter estimation ..... 111
Passivation ..... 64
Passivity ..... 9
Performance ..... 78
Phosphorized copper anodes ..... 1
Photoelectrochemical etching ..... 25
Platinum electrode ..... 56
Plutonium ..... 135,143
Plutonium dioxide ..... 120
Polarization of Ag electrodes ..... 40
Porous electrode ..... 87
Precipitation ..... 87
Pulsed column ..... 143
Pumping loss ..... 104
Purex process ..... 143

R

Radioactive decontamination ..... 156
Radioactive waste ..... 149
Raney nickel ..... 34
Redox-flow battery ..... 104
Reduction ..... 34
Rotating disk ..... 25
Rotating hemispherical electrode ..... 15,111

S

Scale-up parameters ..... 104
Semiconductor electrodes ..... 25
Separation process ..... 143
Separations ..... 135
Shunt current loss ..... 104
Silver catalyst ..... 120
Simplex method ..... 111
Solid electrolytes ..... 40
Solvent extraction ..... 143
Stainless steel ..... 128
Surface diffusion ..... 56
Surface prepolishing ..... 156

U

Uranium ..... 128,135,143

V

Voltage losses ..... 92

Z

Zinc dissolution ..... 9
Zirconia electrochemical cell ..... 56

## CONTENTS


FOREWORD ..... iii

KINETICS OF COPPER DISSOLUTION AT OXYGEN FREE AND PHOSPHORIZED ANODES ..... J.D. Reid and A.P. David 1

MODELING OF ANODIC DISSOLUTION AND PASSIVATION PROCESSES ..... Geoffrey Prentice and Yu-Chi Chang 9

CORROSION OF ZINC BY BROMINE UNDER FLOW CONDITIONS ..... Shih-Liang Chiu and J. Robert Selman 15

A MATHEMATICAL MODEL FOR THE PHOTOELECTROCHEMICAL ETCHING OF SEMICONDUCTORS ..... Mark E. Orazem 25

THE ELECTROCHEMICAL HYDROGENATION OF ORGANIC COMPOUNDS ON RANEY-TYPE METAL CATALYSTS ..... P.N. Pintauro, N. Phan, M.M. Baizer and K. Nobe 34

CATALYTIC AND ELECTROCATALYTIC OXIDATION OF METHANE. POLARIZATION OF SILVER ELECTRODES ..... Savvas Seimanides, Michael Stoukides and Albert Robbat 40

A MATHEMATICAL APPROACH FOR EVALUATING NICKEL-HYDROGEN CELLS ..... Harold F. Leibecki 46

SURFACE DIFFUSION LIMITED OXYGEN EXCHANGE IN ZIRCONIA ELECTROCHEMICAL CELLS ..... Neil L. Robertson and James N. Michaels 56

MODELING OF ELECTROCHEMICAL OSCILLATIONS RELATED TO PASSIVATION: COUPLING OF KINETICS AND DIFFUSION ..... Jan B. Talbot and R.A. Oriani 64

PHENOMENOLOGICAL DISCHARGE VOLTAGE MODEL FOR LEAD-ACID BATTERIES ..... Emile Hyman, William C. Spindler and Jon F. Fatula 78

ELECTROCHEMICAL IMPREGNATION OF POROUS NICKEL HYDROXIDE ELECTRODE ..... Kuo-Chuan Ho and Jacob Jorne 87

AN EMPIRICAL MODELLING APPROACH TO DESIGNING A BATTERY ..... H. Gu, R.L. Galyen and G. W. Brutchen 92

SIMULATION OF A RECHARGEABLE HYDROGEN-BROMINE SPE FUEL CELL ..... S.D. Fritts and R.F. Savinell 96

NUMERICAL ANALYSIS ON SHUNT CURRENT AND PUMPING LOSS IN A REDOX-FLOW CELL SYSTEM ..... K. Kanari, K. Nozaki and T. Ozawa 104

CALCULATION OF CORROSION RATE DISTRIBUTION OF A ROTATING METAL HEMISPHERE ..... Shih-Liang Chiu and J. Robert Selman 111

ELECTROCHEMICAL PROCESS FOR DISSOLVING PLUTONIUM DIOXIDE AND LEACHING PLUTONIUM FROM SCRAP OR WASTES ..... L.A. Bray, J.L. Ryan and E.J. Wheelwright 120

ELECTROLYTIC DISSOLUTION EXPERIENCE AT THE IDAHO CHEMICAL PROCESSING PLANT ..... Stephen J. Dukas, Douglas M. Black, Lloyd W. McClure and Gary F. Offutt 128

THE APPLICATION OF ELECTROREFINING FOR RECOVERY AND PURIFICATION OF FUEL DISCHARGED FROM THE INTEGRAL FAST REACTOR ..... L. Burris, R.K. Steunenberg and W.E. Miller 135

EXPERIENCES WITH ELECTROREDOX EQUIPMENT FOR THE SEPARATION OF PLUTONIUM ..... H. Schmieder and H. Goldacker 143

ELECTROCHEMICAL PROCESSING OF ALKALINE NITRATE AND NITRITE SOLUTIONS ..... D.T. Hobbs and M.A. Ebra 149

ELECTROPOLISHING APPLICATIONS IN THE NUCLEAR INDUSTRY ..... Richard P. Allen 156

# KINETICS OF COPPER DISSOLUTION AT OXYGEN FREE AND PHOSPHORIZED ANODES

J.D. Reid and A.P. David ■ IBM Corporation, 1701 North Street, Endicott, NY 13760

The steady-state current potential and impedance characteristics of copper disk electrodes submerged in typical sulfuric acid cupric sulfate plating solutions were studied. A single charge transfer step limits the dissolution rate over a wide range of interfacial current densities and solution agitation conditions at pure and oxygen free copper anodes. At phosphorized anodes, two kinetic steps contribute to limit the overall dissolution rate under most conditions. Addition of polyethylene glycol and chloride ion to a solution polarized the dissolution process at each of the anode materials. Polarization appeared to result from formation of an adsorbed barrier to diffusion of dissolved ions from the interface, rather than a change in the dissolution mechanism.

## SCOPE

All industrial electrodeposition processes involve a concurrent anodic dissolution reaction, usually involving the same metal or alloy being deposited. Within the printed circuit industry electrolytic copper deposition and dissolution processes are used extensively for formation of conductive surfaces. Composition of the copper anodes used in these processes is usually a relatively pure "oxygen-free" copper or a copper containing a substantial atomic percent of phosphorous. Little fundamental work has appeared regarding dissolution kinetics at these anodes. An improved understanding of the fundamental differences between electrolytic dissolution of oxygen-free and phosphorized copper anodes should serve to improve the basis upon which anodes are selected for a given deposition process. This is particularly relevant considering the recent industry trend toward acid copper electroplating for which phosphorized copper anodes are usually recommended.

## INTRODUCTION

The kinetics of copper dissolution in sulfuric acid have been extensively studied since the early 1950's (1-4). It is generally agreed that the charge transfer reaction:

$$Cu^{2+} + e^- \longleftrightarrow Cu^+$$

limits the deposition or dissolution rate under most conditions. A relatively fast charge transfer or surface diffusion step involving the reaction:

$$Cu^+ + e^- \longleftrightarrow Cu$$

usually influences the overall reaction rate only near the open circuit potential. It has been suggested that two charge transfer reactions as well as a surface transport step are involved in the overall reaction under low overpotential conditions (5,6).

Electrolytic copper deposition processes involving a concurrent dissolution process at a copper anode are presently of great importance in the printed circuit industry. While cathodic kinetic processes are most directly involved in the formation of acceptable copper deposits, anodic kinetics are also important in determining total power consumption and the extent to which anodic oxidation of organic additive species occurs. Anodes utilized in these processes have traditionally been a highly refined "oxygen free" copper or a "phosphorized" copper containing between 0.02 and 0.08 percent phosphorous (7). Relatively little work has appeared regarding the dissolution kinetics of these commonly used anodes, especially in the presence of the organic additives frequently found in the electroplating baths.

AC impedance measurements are easily applied to the determination of kinetic parameters of steady state processes, and have previously been utilized in the study of copper dissolution and deposition (8-10). We have therefore used these measurements, along with steady state current-potential characteristics of a rotating disc copper electrode, to investigate dissolution kinetics at typical copper anodes.

Steady state current potential relations at the rotating disc electrode were interpreted in terms of the Levich and Tafel equations, which have been described extensively elsewhere (11). Impedance data were analyzed using the equivalent circuit shown in Figure 1. A typical dual semicircle impedance plane or Nyquist plot (IPP) of the impedance data usually associated with this circuit is also shown. In this model (12), R1 represents the charge transfer resistance of the $Cu^{2+} \longleftrightarrow Cu^{+}$ reaction and C1 is the associated double layer capacitance. R2 is the resistance limiting the $Cu^{+} \longleftrightarrow Cu(0)$ charge transfer and C2 is the associated capacitance. The dual parallel RC network equivalent circuit model was chosen as the most easily utilized representation of the two step dissolution of copper. As is generally true of equivalent circuit models, values of the R and C parameters may differ from realistic physical values when the model differs from the true system in any way.

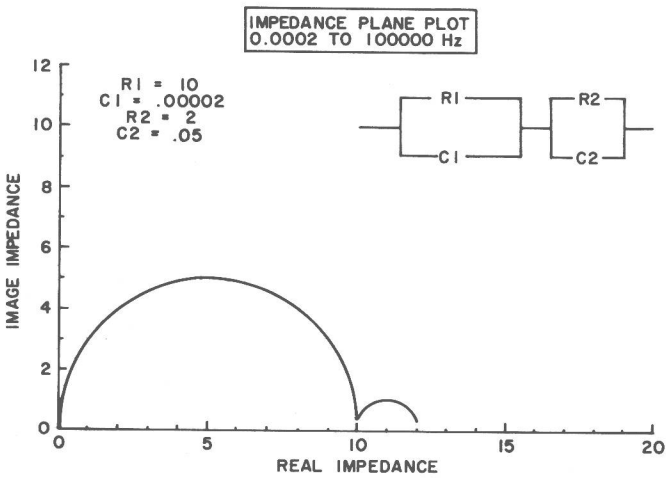


Figure 1. Equivalent circuit diagram and associated impedance plane plot used as a model of copper dissolution kinetics.

## EXPERIMENTAL

Impedances were measured, as previously described (13) using a frequency response analyzer, a potentiostat, and a standard lab computer. A custom made glass cell, utilizing a Luggin capillary, allowed accurate interfacial potential control with the three-electrode system. All potentials were measured and are reported relative to the mercury/ mercury sulfate/satd. potassium sulfate reference electrode. Steady-state interfacial currents were monitored with a low impedance ammeter connected in series with the counter electrode and the potentiostat and were recorded on an X-Y chart recorder.

An AC amplitude of 0.005 V RMS or smaller was used in all studies. The AC amplitude was chosen so that AC current was less than two percent of DC current at any potential. Measured impedances were not strongly influenced by the AC signal amplitude in reported studies.

The electrolyte in all studies, except as otherwise specified, was 0.2 M $CuSO_4$ dissolved in 1.8 M $H_2SO_4$. Reagent grade or better copper sulfate pentahydrate and sulfuric acid were used in all studies. Solutions were equilibrated with ambient atmospheric conditions.

All studies used epoxy shrouded custom machined solid copper rotating disc electrodes of 0.4 $cm^2$ area. Electrode materials were pure copper (99.999%), standard oxygen free anode copper, and an anode containing 0.05 percent phosphorous. Prior to any impedance measurements, steady state currents were allowed to equilibrate at a given potential for at least five minutes. An electrode rotation rate of 500 RPM was used except as otherwise noted.

## RESULTS AND DISCUSSION

### Steady State Current - Potential Characteristics

Steady-state current potential relationships for dissolution of oxygen free, pure, and phosphorized copper anode materials are shown in Figure 2. Each of the electrode materials exhibit nearly identical polarization curves at current densities of less than 100 $mA/cm^2$. At higher current densities, the pure and oxygen free materials continue to show similar behavior, but dissolution of the phosphorized anode occurs at increasingly

polarized potentials. A black film usually became visible on the phosphorized electrode during dissolution, while the oxygen free and pure copper surfaces continued to have a crystalline metallic appearance. This film may have been involved in increasing the phosphorized electrode polarization through either physical blockage of dissolution sites or by increasing the $Cu^+$ or $Cu^{2+}$ concentration at the interface. At current densities of less than 10 mA/cm$^2$ a reproducible ($\pm$ 10%) steady-state potential or current was not reached within five minutes.

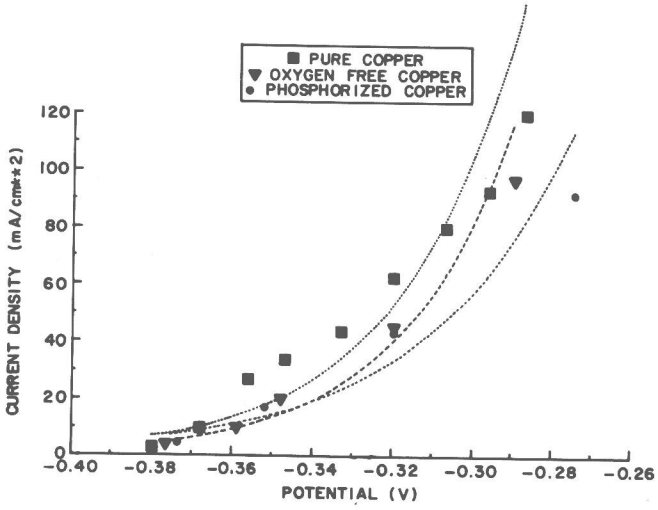


Figure 2. Steady-state current potential relationships for dissolution of copper at a rotating disc electrode submerged in the standard sulfuric acid-cupric sulfate electrolyte.

A relatively insignificant dependence of copper dissolution current density upon electrode rotation rate was observed in all systems studies except when electrode passivation or film formation occurred at lower rotation rates. Figure 3 shows a typical Levich plot measured at phosphorized copper at potentials of -0.18, -0.24, and -0.31 V using rotation rates between 100 and 6000 RPM. At each of these potentials, interfacial currents were only 5 to 15% greater at 6000 RPM than at 100 RPM. Over a wide current density range, the overall copper dissolution rate is determined largely by Cu or $Cu^+$ oxidation charge transfer kinetics from the unit activity solid regardless of mass-transfer effects associated with solution agitation. The small dependence of dissolution current upon rotation rate which was observed may be the result of both a reverse (reduction) reaction involving the high $Cu^+$ concentration near the interface and a shift in the instantaneous rest potential. A cathodic rest potential shift would result in an increased effective applied overpotential for any measured potential. The instantaneous rest potential may become more cathodic at high rotation rates as the cupric ions which are generated are removed more rapidly from the interface. It is well known that the rest potential of a copper electrode in copper sulfate obeys an approximately Nernstian relation over a wide interfacial cupric ion concentration range.

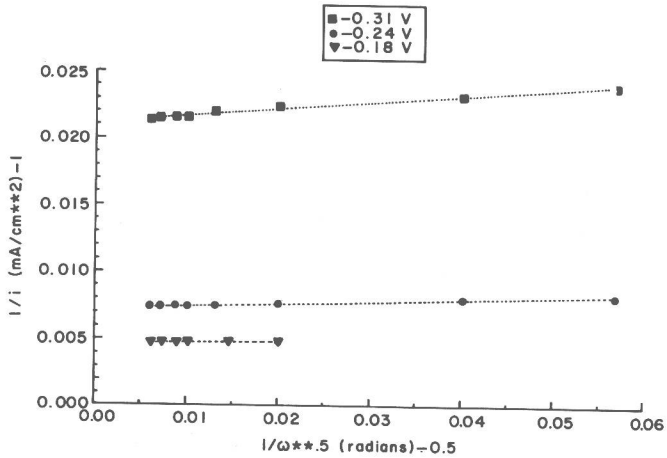


Figure 3. Levich plots of copper dissolution measured at phosphorized copper using electrode rotation rates between 100 and 6000 RPM.

Tafel plots constructed from Levich plot extrapolations of limiting current densities are shown in Figure 4 for pure and phosphorized copper. Over the potential range shown neither mass transfer nor cathodic back reactions should contribute measured results. In both cases, however, considerable curvature of the plots is evident and interpretation of the data is difficult. Observation of the phosphorized electrode surface suggests that formation of a film or precipitate layer, especially at the higher overpotentials, introduced a physical barrier to current flow not accounted for by the Tafel model. Using the linear fits to the data at lower overpotentials shown in Figure 4, exchange currents of 11 and 7 mA/cm$^2$ are calculated for the pure and phosphorized copper

respectively. An inverse Tafel slope of 120 mV/decade and a transfer coefficient of $\alpha = 0.5$ are determined for both phosphorized and pure copper. The exchange currents are in reasonable agreement with those supported previously (1,5). The Tafel slope and the transfer coefficient do not agree well with typical reported values of 40 mV/decade and $\alpha = 1.5$, possibly as a result of the potential region over which the Tafel lines were drawn.

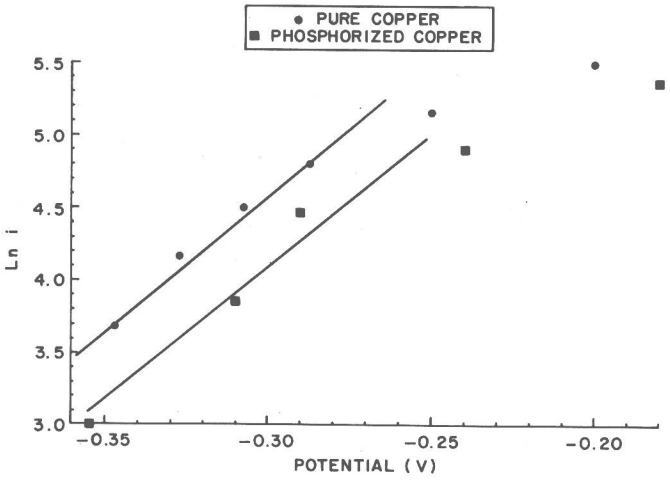


Figure 4. Tafel plots of anodic copper dissolution constructed from limiting current estimated from Levich plot extrapolations.

An upper limit to the current density was set by formation of a passivating $CuSO_4$ precipitate film at the interface. Upon formation of the precipitate, the current dropped to zero at potentials within the 10V output limit of the potentiostat. Figure 5 shows Levich type plots of the maximum steady state current (not generating a passivating film) as a function of the electrode rotation rate. The phosphorized and pure copper anode materials are nearly identical with respect to passivating film formation. For each anode a maximum steady state current of about 100 mA/cm$^2$ is possible at 100 RPM, while at 1600 RPM the maximum current is 200 mA/cm$^2$. The linear Levich plot indicates that a copper sulfate film, the dissolution of which is dependent on interfacial solution flow, is largely responsible for passivation. It was found that passivation occurred at lower current densities with increasing bath sulfuric acid or copper sulfate concentrations, in agreement with cupric sulfate precipitate film formation mechanism. It should be noted that the Levich plots do not extrapolate to 1/i = 0 at 1/w = 0, as would be anticipated if copper sulfate precipitation were the only passivation mechanism. This suggests that a precipitate such as a thermodynamically unstable cupric oxide may also form at the interface, independent of the electrode rotation rate.

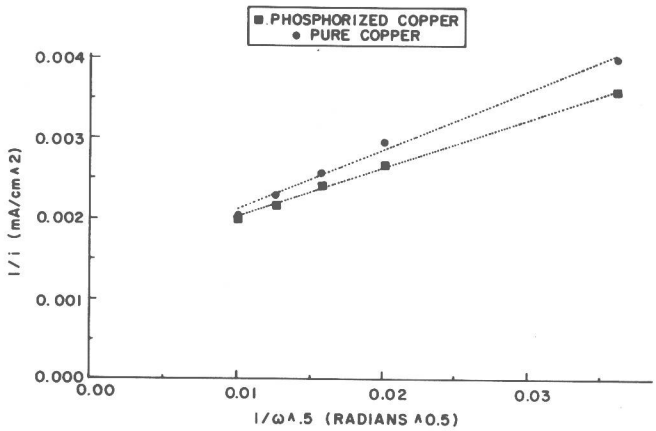


Figure 5. Levich plots of the maximum achievable steady-state current density not resulting in copper passivation as a function of electrode rotation rate.

As shown in Figure 6, the addition of 300 ppm polyethylene glycol along with 35 ppm chloride ion to the acid copper solution results in a substantial (25 to 75 mV) polarization of the copper anodes. Previous studies (14,15) have suggested that many polymers, including PEG, adsorb at and polarize the copper cathode interface. The effect has been attributed to formation of a stabilized $Cu^+$ intermediate and to formation of a film through which diffusion of the cupric ion to the interface is inhibited. The polarizing effect of PEG-$Cl^-$ adsorption was most pronounced at the oxygen free and pure copper electrodes in comparison to the effect at phosphorized anodes. The origin of this difference is unclear, but the presence of copper phosphate species at the interface may act to inhibit adsorption of the polarizing PEG-$Cl^-$ layer. Adsorption of PEG in the absence of $Cl^-$ polarized the interface by only 5 to 20 mV and $Cl^-$ alone had no detectable effect at 35 ppm concentrations.

This suggests the formation of a strongly adsorbed Cl-PEG complex or enhanced adsorption of PEG upon sites at which $Cl^-$ is adsorbed at the interface.

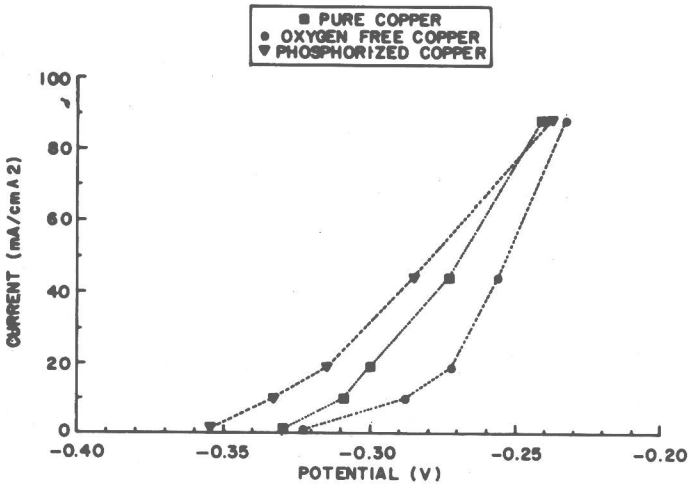


Figure 6. Steady-state current potential relationships for copper dissolution in the presence of 300 ppm PEG and 35 ppm $Cl^-$.

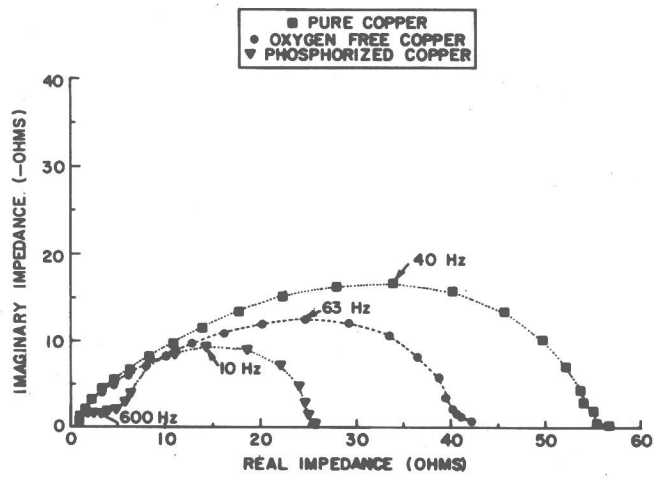


Figure 7. Impedance plane plots measured during 1 mA/cm$^2$ steady-state copper dissolution in the standard acid copper electrolyte.

## Impedance Characteristics

Figure 7 shows impedance plane plots for pure, oxygen free, and phosphorized copper measured at a steady state anodic current density of 1 mA/cm$^2$. Over the frequency range studied (0.4 to 60,000 Hz) a single depressed semicircle is observed for both oxygen free and pure copper. We interpret the appearance of this single semicircle as indicating dissolution rate control involving a single charge transfer step at an inhomogeneous electrode surface. At phosphorized copper, the resolution of two semicircles indicates that two distinct physical steps contribute significantly to limiting the dissolution rate.

The width, in Ohms, of the semicircles on the real impedance axis is equal to the effective charge or mass transfer resistance of each reaction. Capacitances associated with the IPP semicircles are calculated using the relation $\tau = 1/w = RC$, where R is the width and $\tau$ is the time constant of the semicircle.

Oxygen-free and pure copper IPP's yield charge transfer resistances of 16 and 21 $\Omega$/cm$^2$ respectively. In each case, an interfacial capacitance of approximately 150 uF/cm$^2$ is calculated. This value is

within the range associated with compact layer charge separation at a rough metallic surface in a concentrated electrolyte.

At phosphorized copper resistances of 8 and 3 $\Omega/cm^2$ and associated capacitances of 2000 and 150 $uF/cm^2$ are determined from the IPP semicircles. The higher frequency semicircle (3 $\Omega/cm^2$ - 150 $uF/cm^2$) appears to correspond to a charge transfer coupled in parallel with a compact layer capacitance as described for pure and oxygen-free copper. The lower frequency semicircle yields a capacitance of 2000 $uF/cm^2$, a value larger than those normally associated with electrode processes. Such a high capacitance could originate from rapid generation and recombination of $Cu^+$ within a very small plane ($\sim 10^{-10}$ M) at the copper surface.

Figures 8 and 9 show IPP's measured at the copper anodes during steady-state current densities of 9 and 85 $mA/cm^2$ respectively. As was observed at 1 $mA/cm^2$, two semicircles are resolved at phosphorized copper while only one feature is resolved at the pure and oxygen free copper. Dissolution of phosphorized copper appears to be a two step process over a wide current density range, while dissolution of pure and oxygen-free copper is limited by a single charge transfer step.

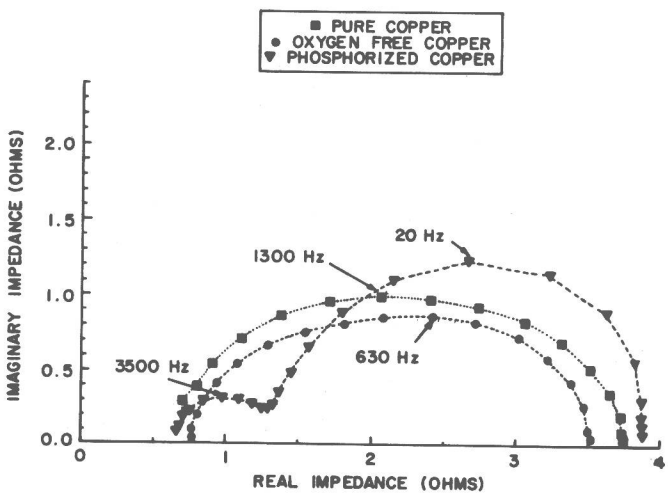


Figure 8. Impedance plane plots measured during 9 $mA/cm^2$ steady-state copper dissolution in the standard acid copper electrolyte.

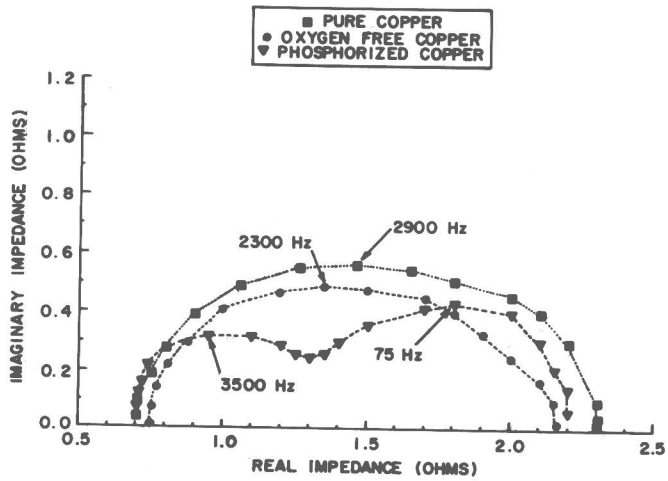


Figure 9. Impedance plane plots measured during 85 $mA/cm^2$ steady-state copper dissolution in the standard acid copper electrolyte.

As shown in Figure 10, effective charge transfer resistances, as determined from IPP semicircle widths, decrease sharply with increasing overpotential or current as is anticipated for reactions with an approximately exponential dependence on potential. It is of interest to note that for phosphorized copper the relative resistance of the high frequency semicircle to that of the low frequency semicircle increased at higher currents. This suggests that the $Cu^{2+} \longleftrightarrow Cu^+$ reaction (associated with the high frequency semicircle) becomes increasingly important in limiting the dissolution rate as the current is increased. At lower currents, the reaction rate is largely determined by the $Cu \longleftrightarrow Cu^+$ generation process associated with low frequency semicircle. Previous studies at various copper substrates have concluded that the $Cu^{2+} \longleftrightarrow Cu^+$ reaction is rate limiting except at very low current densities. At oxygen-free and pure copper, where a single high frequency semicircle is resolved, it appears that the $Cu^{2+} \longleftrightarrow Cu^+$ reaction is rate limiting over the entire current density range studied.

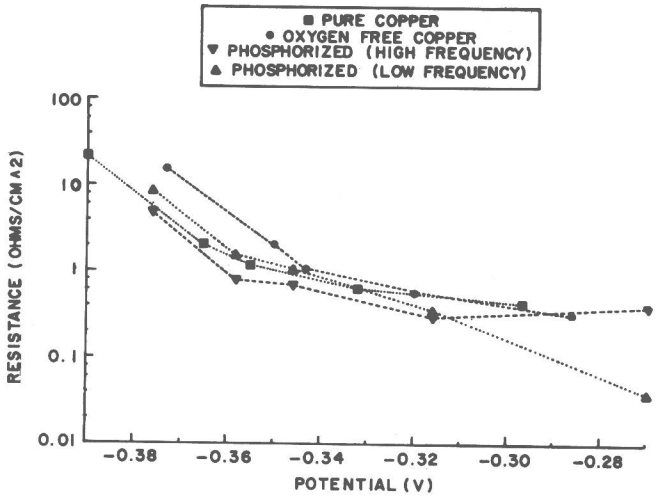


Figure 10. Effective charge transfer resistances for copper dissolution as a function of applied potential.

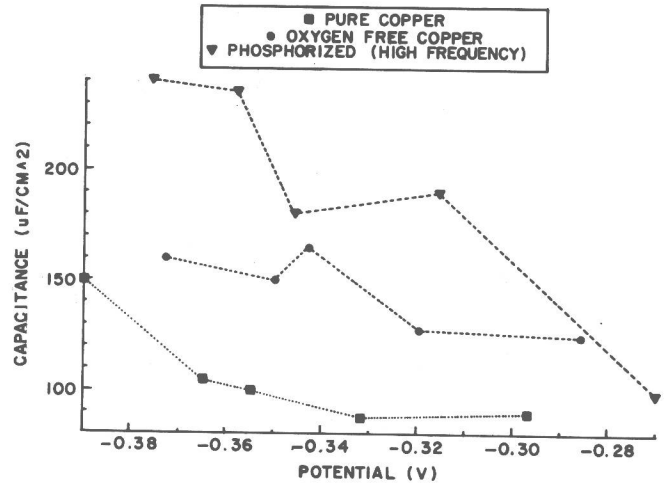


Figure 11. Interfacial capacitance as a function of potential during copper dissolution in the standard electrolyte.

Exchange currents of 1.1, 1.3, and 1.7 $mA/cm^2$ for pure, oxygen-free, and phosphorized copper respectively were determined from rest potential impedance data using the relation:

$$i_o = RT/nFR_{ct}$$

where F is Faraday constant, T is temperature, n is electrons per molecule oxidized, R is the gas constant, and $R_{ct}$ is the charge transfer resistance. The values are somewhat lower than those determined from Tafel plot extrapolations but are within the range previously reported for copper in sulfuric acid (1,5).

Double layer capacitances, determined from IPP semicircles, are shown as a function of potential in Figure 11. The general decrease of values with increasing overpotential is thought to reflect a decrease in anode surface area or roughness at higher currents. Capacitance differences between different anodes likewise suggest that steady-state surface area at the phosphorized copper is generally greater than at pure or oxygen-free copper. The data suggests a potential independent compact layer, rather than a Gouy-Chapmann layer (which should show a capacitance increase with increasing potential). The capacitance calculated from the low frequency phosphorous semicircle remain in the range of 2000 to 6000 $uF/cm^2$ over the potential range studied.

Upon addition of 300 ppm PEG and 35 ppm $Cl^-$ to the base acid copper electrolyte, charge transfer resistances measured at a given overpotential increased substantially. The increasingly polarized current-potential curves (Figure 6) observed in the presence of PEG-$Cl^-$ are a manifestation of this increased charge transfer resistance. At oxygen-free and pure copper, the general impedance characteristics were not otherwise changed. Generally, the IPP's measured at a larger overpotential in the presence of PEG-$Cl^-$ were identical to those obtained at a lower overpotential in the base system. This behavior indicates that the effect of PEG-$Cl^-$ additions is to slow the kinetics of the rate limiting step, but not to change the nature of the step. A diffusional barrier mechanism of rate limitation, rather than one involving $Cu^{2+}$ or $Cu^+$ complexation is suggested by the unchanged nature of the impedance behavior.

Phosphorized copper impedance behavior in the presence of PEG-$Cl^-$ was altered considerably. At all potentials the "high frequency" semicircle associated with double layer capacitance was resolved, however only within the 15 to 25 $mA/cm^2$ current density range was a second semicircle (low frequency - high capacitance) resolved. PEG-$Cl^-$ adsorption appears to have selectively inhibited the charge transfer associated with the high frequency semicircle, thus making this feature dominant in the IPP.

The addition of sulfonated or mercapto "brightener" species to the acid copper system resulted in the resolution of two IPP semicircles at pure, oxygen-free, and phosphorized copper. The altered impedance behavior indicates that these species adsorb at the anode as well as at the cathode in acid copper baths. Since molecules with pendant sulfur atoms generally exhibit very high affinity for $Cu^+$, it would be expected that these molecules would be largely present as complexes with $Cu^+$ at the surface. The second IPP semicircle resolved in this case probably corresponds to a charge transfer reaction involving a stabilized mercapto-cuprous complex.

## CONCLUSIONS AND SIGNIFICANCE

During steady-state anodic copper dissolution conditions typical of production acid copper plating baths the dissolution rate is limited by kinetic rather than diffusional or convection processes. The kinetics of dissolution determine the anodic overpotential associated with any plating current and thus influence total power consumption and the oxidation of any organic species present in the bath. As anodic current densities are increased above 100 $mA/cm^2$ diffusion of cupric ion away from the interface begins to limit the overall dissolution rate in the absence of substantial convection. Formation of a passivating cupric sulfate film at the anode occurs at a current density which decreases with decreasing solution convection. Passivation of anodes in plating baths results in marked increases of organic additive oxidation as well as power consumption. The steady-state dissolution kinetics of oxygen free, phosphorized, and pure copper anodes were generally similar. Each of the anodes was polarized to some extent by the addition of the typical bath constituents polyethylene glycol and chloride ion to solution. Dissolution at the oxygen free and pure copper anodes appeared to be controlled by a single kinetic step, while two kinetic steps contributed to limiting dissolution at phosphorized anodes.

## LITERATURE CITED

1. Bockris, J. O'M. and M. Enyo, "Trans. Faraday Soc.," 58, 1187 (1962).
2. Mattsson, E. and J. O'M. Bockris, "Trans. Faraday Soc.," 55, 1586 (1959).
3. Demedts, G. and A. P. Van Peteghem, "Corrosion Sci.," 18, 1041 (1978).
4. Bockris, J. O'M. and H. Kita, "J. Electrochem. Soc.," 109, 928 (1962).
5. Kita, H., M. Enyo and J. O'M. Bockris, "Can. J. Chem.," 39, 1670 (1961).
6. Hurlen, T., G. Ottesen and A. Staurset, "Electrochimica Acta," 23, 39 (1978).
7. Thompson, E. W., "Trans. Inst. Metal Finishing," 59, 30 (1981).
8. Burrows, I. R., J. A. Harrison, J. Thompson, "J. Electroanal. Chem.," 58, 241 (1975).
9. Pearson, I. M., G. F. Schrader, "Electrochimica Acta," 13, 2021 (1968).
10. Gorbundova, K. M. and Z. A. Tkachik, "Electrochimica Acta," 16, 191 (1971).
11. Bard, A. J. and L. A. Faulkner, Electrochemical Methods, John Wiley and Sons, New York, 1980.
12. Reid, J. D. and A. P. David, Proceedings of Electrochemical Society Fall Meeting, p339, Las Vegas, NV, Oct., 1985.
13. Reid, J. D., P. Vanysek and R. P. Buck, "J. Electroanal. Chem.," 170, 109 (1984).
14. Yokio, M., S. Konishi, T. Hayashi, "Denki Kagaku," 52, 218 (1984).
15. Molendar, A. and J. Brown, "Plating," 51, 649 (1974).